Characterization and Application of Nanomaterials 2024, 7(1), 5756.
https://doi.org/10.24294/can.v7i1.5756

Article

Enhanced photocatalytic performance by ZnO/Graphene heterojunction grown on Ni foam for methylene blue removal

Lucas F. Melia[1], María V. Gallegos[2], Luciana Juncal[1], Marcos Meyer[1], Francisco J. Ibañez[3], Laura C. Damonte[1,*]

[1] Instituto de Física La Plata (IFLP), CONICET-UNLP, La Plata 1900, Argentina
[2] Centro de Investigación y Desarrollo en Ciencias Aplicadas (CINDECA), CONICET-UNLP-CIC, La Plata 1900, Argentina
[3] Instituto de Investigaciones Fisicoquímicas, Teóricas y Aplicadas (INIFTA), Universidad Nacional de La Plata-CONICET, La Plata 1900, Argentina
*** Corresponding author:** Laura C. Damonte, damonte@fisica.unlp.edu.ar

CITATION

Melia LF, Gallegos MV, Juncal L, et al. Enhanced photocatalytic performance by ZnO/Graphene heterojunction grown on Ni foam for methylene blue removal. Characterization and Application of Nanomaterials. 2024; 7(1): 5756. https://doi.org/10.24294/can.v7i1.5756

ARTICLE INFO

Received: 15 April 2024
Accepted: 30 April 2024
Available online: 29 May 2024

Abstract: ZnO nanostructures were obtained by electrodeposition on Ni foam, where graphene was previously grown by chemical vapor deposition (CVD). The resulting heterostructures were characterized by X-ray diffraction and SEM microscopy, and their potential application as a catalyst for the photodegradation of methylene blue (MB) was evaluated. The incorporation of graphene to the Ni substrate increases the amount of deposited ZnO at low potentials in comparison to bare Ni. SEM images show homogeneous growth of ZnO on Ni/G but not on bare Ni foam. A percent removal of almost 60% of MB was achieved by the Ni/G/ZnO sample, which represents a double quantity than the other catalysts proved in this work. The synergistic effects of ZnO-graphene heterojunctions play a key role in achieving better adsorption and photocatalytic performance. The results demonstrate the ease of depositing ZnO on seedless graphene by electrodeposition. The use of the film as a photocatalyst delivers interesting and competitive removal percentages for a potentially scalable degradation process enhanced by a non-toxic compound such as graphene.

Keywords: Ni foam; electrodeposition; zinc oxide; photocatalysis; graphene; methylene blue degradation

1. Introduction

It is known that water pollution is an environmental problem that worsens year after year. Human activities, such as industry and agricultural production, affect bodies of water and, consequently, human health [1]. It is believed that of all wastewaters generated by human activities, 80% are discharged without prior treatment. Poor-quality drinking water is a problem that is associated with 80% of childhood illnesses and 50% of child deaths worldwide [2]. Among water contaminants, organic dyes play a leading role: around 100,000 different types of dyes are produced annually, totaling more than 700,000 tons, with approximately 100 tons being dumped [3,4]. In addition to many of them being carcinogenic and dangerous for humans [5,6], they have good stability in environmental conditions [7] and cause, among other drawbacks, loss of transparency, reduction in the penetration of sunlight, retard biological activity of plants and animals, increase chemical oxygen demand (COD) and biochemical oxygen demand (BOD), etc. [8,9]. In this context, organic dyes contribute significantly to this environmental problem since they are one of the main sources of contamination of surface and groundwater [10]. One of the most commonly used dyes is methylene blue (MB). MB, from the thiazine class, is a heterocyclic aromatic compound; see **Figure**

1 [11]. This cationic dye is commonly used in the textile industry to dye wool, cotton, etc., where 15% is transferred to wastewater during this process as an industrial pollutant [12–14]. These dyes have also long been used in medicine and scientific purposes, such as in microscopy or as redox indicators [15]. Although this dye can be used as a drug against some diseases, such as malaria, it is also toxic to human health and the environment and can cause vomiting, nausea, irritation, and tachycardia, among other diseases, in humans. This pollutant can inhibit plant growth and reduce the pigment and protein content of algae [16–18]. For these reasons, the elimination of these pollutants from water is now one of the main areas of study [3].

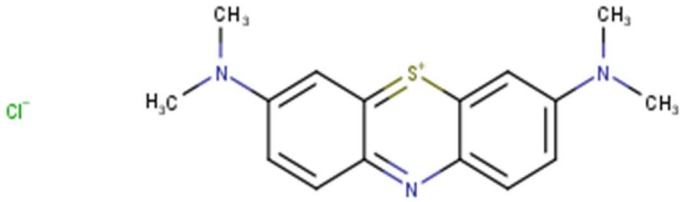

Figure 1. Schematic representation of methylene blue (MB) dye.

The removal mechanisms of MB and other contaminants from wastewater are frequently studied [19–21]. Photodegradation via photocatalysis using semiconductors is a preferred way to eliminate contaminants in various sources of water [22,23]. One of the main advantages of photocatalysis relies on the generation of non-harmful products, such as CO_2, H_2O, and inorganic salts, after activating the process with light [24,25]. Although there are various kinds of semiconductors that adapt well to these systems, including Fe_2O_3, CdS, and ZnS [3], TiO_2 and ZnO are the most used in photocatalysis applications [10]. Most likely due to their low toxicity, outstanding thermal and chemical stability, and relatively low cost [26]. In particular, ZnO presents higher percentages of contaminants degradation in water than TiO_2 [27], which could be due to the higher exciton binding energy and the higher electrical conductivity of ZnO compared to TiO_2, in addition to the ZnO band potentials (of valence and conduction) being lower than TiO_2 ones. This combination of properties allows an increase in the effectiveness of the degradation reactions [28,29]. In this context, the use of thinly supported ZnO films is most desired since it allows a very simple separation process, which consists of removing the catalyst from the solution and also facilitating the recycling of the catalyst. On the other hand, the use of ZnO powder involves separation by some subsequent process. In addition to this, it is known that the photodegradation efficiency increases as the specific surface increases [30]. This is why the use of porous supports, such as nickel foams, can obtain very high performance, comparable to powders.

ZnO thin films can be obtained through various methods, such as metal-organic chemical vapor deposition (CVD) [31,32], magnetron sputtering [33,34], molecular-beam epitaxy [35,36], sol-gel [37], spray pyrolysis [38,39] and electrodeposition [40–42]. What is interesting about the latter is the simple scalability, film control, and the possibility of depositing structures in many different shapes and sizes without using high temperatures or expensive equipment. Growth can be carried out through various solutions that use Zn^{2+} salts with different anions, whether chlorides, nitrates, or sulfates, as precursors [43–48]. By varying the type, concentration, or pH of these

solutions, as well as the applied potential, the deposition time, or the current circulating in the cell, various types of ZnO films and morphologies can be obtained [49–54]. However, it is desirable to use low currents or voltages, low-concentrated salts with non-toxic precursors, and low times so that the process is profitable and easily scalable.

One of the ways to improve the properties of ZnO is to form heterostructures with graphene. CVD graphene presents outstanding properties such as transparency, flexibility, high carrier mobility, and mechanical stability [55–57]. When graphene is grown in 3D structures, the carbon atoms are exposed on the surface, resulting in a large surface area and a large number of active sites [58]. The three-dimensional ZnO-Graphene heterojunction provides synergetic properties and improves charge separation by ZnO followed by charge transport offered by highly conductive graphene, which dramatically reduces the probability of electron-hole recombination [59,60]. This happens because the work function of graphene (−4.5 eV) is lower than the conduction band of the semiconductor oxide (−4.1 eV), so the excited electrons in ZnO are transported toward graphene, which has a high carrier mobility, thus inhibiting recombination in ZnO and consequently increasing the photocatalysis degradation efficiency of MB [61]. Researchers have shown that the photocatalytic activity of ZnO improves whenever graphene is used as a co-catalyst [62]. In addition, graphene could extend the absorption range of ZnO to longer wavelengths further from the ultraviolet region [59]. These exceptional properties offered by the ZnO-Graphene heterojunction have been applied in various fields, including photocatalysis, photodetection, solar cells, etc.

In this work we propose the electrodeposition of ZnO on graphene already grown on a Ni foam by CVD to be used in photodegradation applications. This heterojunction is interesting both as an adsorbent material and for photocatalysis due to the high specific surface area provided by using Ni foam as a substrate, added to the improvement in conductivity and the decrease in electron/hole recombination provided by graphene.

2. Materials and methods

We proposed to grow ZnO nanostructures by electrodeposition on Ni foam, a low-cost and simple technique that had proved to be successful in obtaining ZnO films on different flat substrates like ITO and FTO [40–43].

2.1. Graphene growth in nickel foam

Nickel foam with 1.6 mm thickness and porosity of 87% was purchased from MTI Corp (Richmond, CA, USA). Graphene was grown on Ni foam by CVD method on Ni foam following the protocol described by Messina et al. [63]. Briefly, the bare Ni foam was sonicated in acetone for 20 min and placed in a quartz tube under a vacuum pressure of 8×10^{-5} torr. During the synthesis, a constant flow of H_2 was maintained at a rate of 75 mL min^{-1}. At 950 °C a flow of CH_4 was introduced at a rate of 35 mL min^{-1} for 5 min leading to the growth of graphene on the entire surface of Ni. Finally, the furnace was cooled down at a rate of 16 °C per minute until reaching room temperature.

2.2. Electrodeposited ZnO films

A thin layer of ZnO was grown on Ni with and without graphene by the electrodeposition technique using a Teq4 potentiostat from NanoTeq, Argentina. The aqueous solution was 0.01 mol/L $Zn(NO_3)_2$ (Sigma Aldrich, 98%) in 0.1 mol/L KCl (Anedra, 99.6%) and 0.1 mol/L KNO_3 (Anedra, 99.8%).

The electrolytic cell is a three-electrode setup where Ni foam, Pt wire, and Ag/AgCl electrodes immersed in 3.0 M KCl acted as working, counter, and reference electrodes, respectively. **Figure 2** shows a scheme of the cell. Before electrodeposition, the working electrode was washed with soapy water, sonicated in distilled water for 10 min, and then sonicated in isopropyl alcohol for 10 min. Electrodeposition was performed at constant temperature (70 ℃) and stirring (200 rpm) to ensure homogenous distribution. The applied voltage was −800 mV (chosen after performing cyclic Voltammetry on the studied system) for 60 min. The initial pH of the solution is 5.3. The samples obtained were called Ni/G (Ni foam + graphene), Ni/ZnO (ZnO on Ni foam), and Ni/G/ZnO (ZnO on Ni foam with graphene).

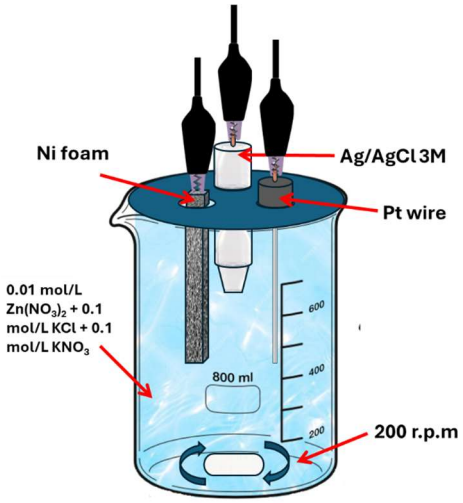

Figure 2. Scheme represents the three-electrode set-up under the parameters used in this work.

2.3. Sample characterization

Cyclic voltammetry and subsequent amperometry were performed using a Teq4 potentiostat from NanoTeq Co., Argentina. X-Ray Diffraction (XRD) patterns were acquired using a Philips PW1710, Panalytical X'Pert PRO diffractometer at 45 kV and 45 mA with monochromatized CuK_α radiation in the range of $20° \leq 2\theta \leq 40°$ with a step of 0.02 °/s and a grazing angle of 3°. Optical images were obtained through a Leica DM IL LED optical microscope. SEM images were obtained from an FEI Quanta 250 environmental scanning microscope (ESEM) at an operating voltage of 20 kV. The equipment has an X-ray detector, EDAX, through which the chemical composition was studied qualitatively using energy dispersive spectroscopy (EDS).

2.4. MB degradation

The photodegradation of MB was evaluated by immersing Ni, Ni/G, Ni/ZnO, and Ni/G/ZnO in 1.3 ppm methylene blue (MB) solution. The solution was kept in the dark

for 15 min to reach adsorption equilibrium. Then, it was irradiated with an 8 W fluorescent lamp (BTE Lighting, Argentina) with a wavelength ranging from 250 to 600 nm. The UV lamp was kept on for 165 min and the experiment was carried out at room temperature. **Figure 3** shows the experimental set-up. At the indicated times, the sample was removed from the solution, and the absorbance of the remaining solution was measured using a Shimadzu UV-2600 spectrometer.

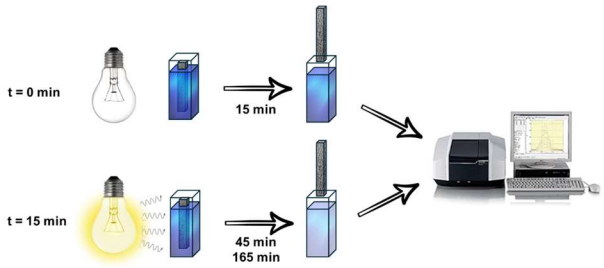

Figure 3. Scheme of the experimental set-up used to measure MB adsorption and degradation.

3. Results

In this section details of the electrodeposition method are presented along with the structural and morphological characterization of the obtained heterostructures. Also, the use of these samples on the MB removal is analyzed.

3.1. Cyclic voltammetry (CV) and amperometry

CVs were run from negative from 0 to −1.1 V and back to 0 V at 100 mV/s scan rate. **Figure 4** shows only the cathodic sweep that is of interest for the ZnO deposition. The CV reveals significant differences based on the electrode substrate. Our group successfully electrodeposited ZnO on different substrates, including ITO and FTO, by applying potentials between −700 mV and −1000 mV. We identified −800 mV as the optimal potential. Therefore, we applied −800 mV which resulted in a noticeable increase in the steep curve for Ni/G as compared to the naked Ni electrode shown in **Figure 4**. Due to the increase in slope observed in both cases, this potential was chosen and applied for 1 h. After amperometry, the Ni/G sample exhibited a white deposit to the naked eye, while no apparent change in color was observed for Ni foam.

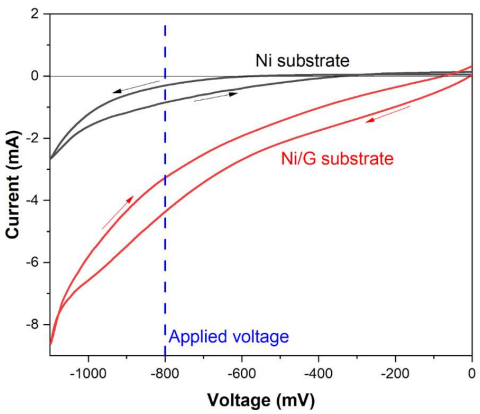

Figure 4. Cyclic Voltagrams corresponding to Ni (black) and Ni/G (red) electrodes.

3.2. X-Ray diffraction (XRD)

Figure 5 shows the diffractograms for Ni/ZnO and Ni/G/ZnO samples measured at angles between 20° and 40°, a region where the characteristic diffraction peaks of ZnO become more evident after smoothing the original signal using the Savitzky-Golay method. Amperometry was performed for 1 h on both samples. As it can be seen, no characteristic peak for ZnO was detected within the Ni/ZnO sample. This does not necessarily rule out the deposition of ZnO since there may be a low amount of mass that is below the limit of detection. On the other hand, for Ni/G/ZnO samples, three peaks clearly evolved, corresponding to (100), (002), and (101) crystallographic orientations that matched the peaks for ICSD no. 01-080-0074. This clearly confirms the successful deposition of the ZnO semiconductor onto the Ni/G sample. Furthermore, there is no evidence of preferential growth in the (002), as the intensity of this peak (at 34.335°) is not dominant. This is consistent with the literature, which has also shown predominant (101) peaks using electrodeposition and other techniques [30,64–66]. These results suggest that the as-deposited ZnO film does not display a nanocolumnar morphology [67]. Additionally, no other diffraction peaks are detected, as Ni exhibits diffraction peaks for $2\theta > 40°$ [68]. The technique also allows us to confirm that no other crystalline material was deposited in large quantities, since the diffractograms do not present other peaks, nor amorphous ones, since no bands were observed at low angles.

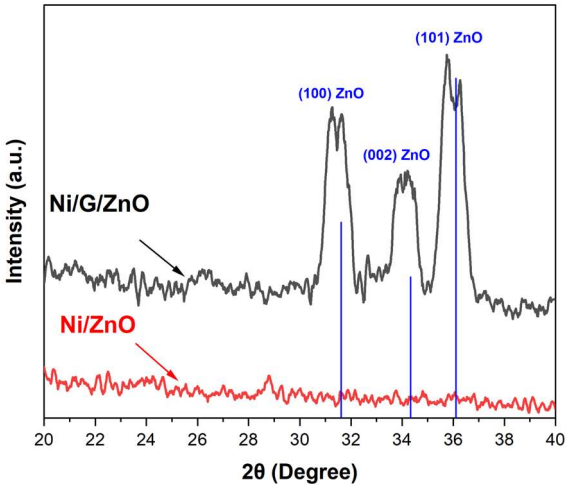

Figure 5. XRD Diffractogram comparing Ni/ZnO and Ni/G/ZnO samples. Blue lines that correspond to card no. 01-080-0074 are used as a comparison.

3.3. Optical microscopy

Figure 6A exhibits multiple pores within the naked Ni foam structure. No apparent changes were detected for graphene grown on Ni foam (not shown), most likely due to the poor resolution of the optical microscope. **Figures 6B** and **6C** clearly exhibits the as-deposited ZnO; however, the amount of deposit seems not to be uniform along the entire Ni/G/ZnO sample.

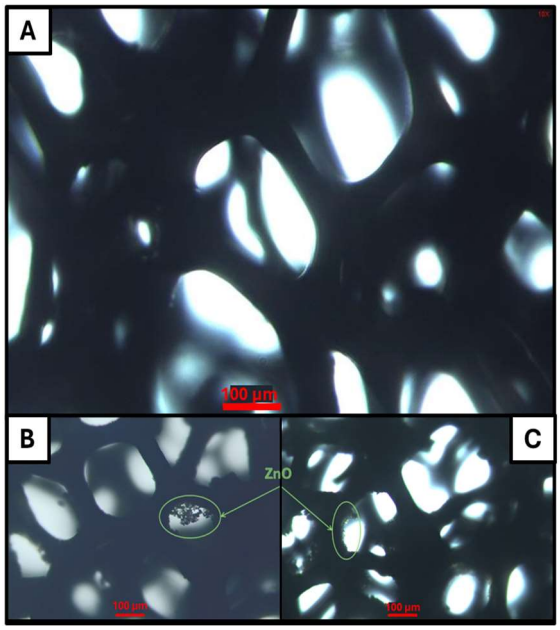

Figure 6. Optical images. **(A)** Ni foam; **(B)** Ni/G/ZnO sample; **(C)** Ni/G/ZnO sample.

3.4. SEM-EDS

Figure 7 shows SEM images for Ni (A), Ni/G (B), Ni/ZnO (C), and Ni/G/ZnO (D). Notable differences in the surfaces are observed between the electrodeposition of ZnO on bare Ni and on Ni/G using the same deposition parameters. **Figure 7B** clearly shows the growth of graphene on the surface of bare Ni. It can be seen there is a large amount of graphene in the center of the foam and that, close to the edge of the pores, that decreases. To confirm that it was a different material, it was analyzed with backscattered electrons, since in this type of image the contrast is based on the atomic number.

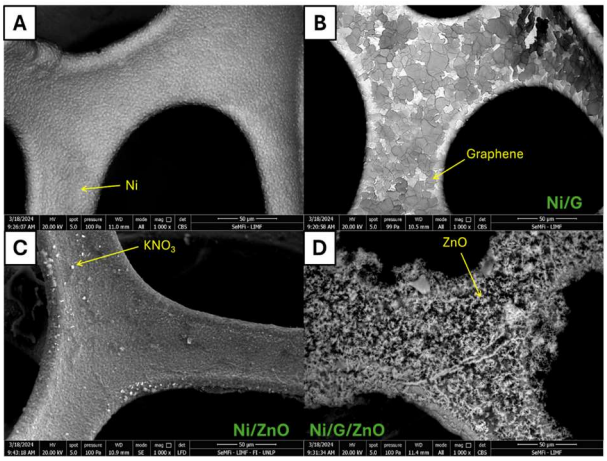

Figure 7. SEM images. **(A)** Ni; **(B)** Ni/G; **(C)** Ni/ZnO; **(D)** Ni/G/ZnO.

Figure 8 shows a SEM image of the Ni/G sample obtained by backscattered electrons. In these images the contrast is achieved with the difference in atomic number, which allows us to confirm that they are two different materials since the Ni substrate appears bright while the graphene deposit appears dark. This confirms that

the CVD deposit was successful.

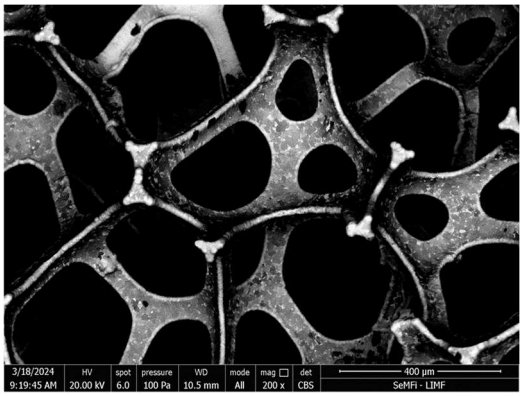

Figure 8. SEM image of the Ni/G sample obtained by backscattered electrons.

On the other hand, the Ni/ZnO sample does not present changes with respect to the Ni sample, except for the appearance of localized structures that are observed as white dots in **Figure 7C**. The amount of Zn provided by EDS in this sample is very low (about 3.5% by weight), consistent with a very low amount of ZnO deposited. As for other elements, the percentage by weight of O, K, N, and Cl revealed 40%, 25%, 13%, and 5% by weight, respectively. The presence of various elements, besides Zn, suggests the potential formation of KNO_3 and KCl crystals that arose during the drying-off process after electrodeposition.

Figure 7D shows the homogeneous growth of ZnO on the Ni/G substrate. EDS measured at various points in the sample indicated 27% and 31% by weight of Zn and O, respectively. In addition, a similar amount of C (31% by weight) was detected, consistent with the growth of graphene. This confirms the successful deposition of ZnO and indicates that graphene remains even after the voltage application in the synthesis. **Figure 9** shows the Ni/G/ZnO sample with a higher magnification, where an increase in the exposed surface can be seen due to the irregularity of the deposit. This type of morphology is comparable to those reported in the literature, despite using a different ZnO deposition technique [64,65]. Finally, **Figure 10** shows a color map obtained by EDS, which shows the location of the evaluated elements. It is confirmed that ZnO is deposited throughout the foam, unlike graphene, which is mostly located in the center of it.

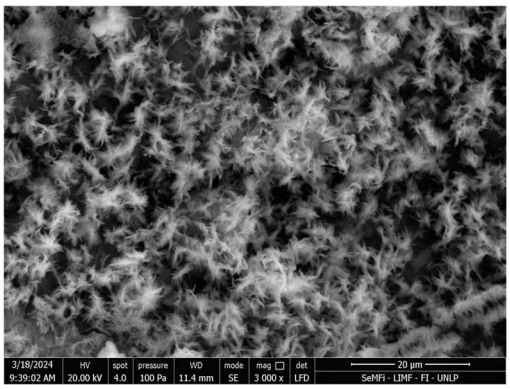

Figure 9. SEM image of the Ni/G/ZnO sample at higher magnification, showing the uniformity of the deposit.

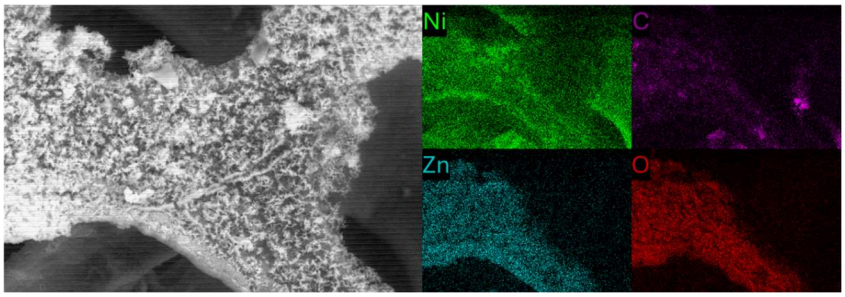

Figure 10. EDS color map showing the location of Ni, C, Zn, and O elements within the Ni/G/ZnO sample.

3.5. Removal of MB from a solution

An absorption spectrum was initially obtained after immersing the samples in 1.3 ppm MB solution for 15 min under dark conditions. In this way, the percentage of MB adsorption in the first min of the experiment was obtained. Then, the lamp was turned on and absorbance measured at 45 and 165 min. To calculate the percentage removal of MB in the solution, we choose to measure the area under the curve for the absorption band located at 662 nm. Finally, Equation (1) was applied to obtain the MB removal percentages:

$$\text{MB Removal [\%]} = (1 - A_t/A_0)\ 100 \quad (1)$$

where A_t is the absorption measured at a certain time t and A_0 is the initial absorbance. **Figure 11** shows the absorbance spectra for each sample measured at the indicated times.

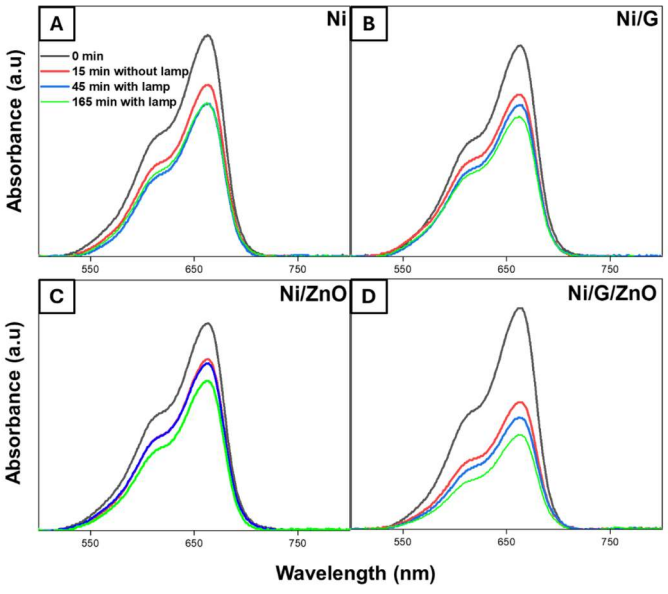

Figure 11. Absorbance spectra of the samples measured at different times: under dark (black curve), after 15 min exposure to light (red curve), after 45 min (blue curve) and 165 min (green curve). **(A)** Ni; **(B)** Ni/G; **(C)** Ni/ZnO; **(D)** Ni/G/ZnO.

Table 1 shows the MB removal percentages for each sample for two different periods of time: while the light was off, that is, the black and red curves indicated in **Figure 11**, and then once the light was turned on, that is, between the red and green curves of the same figure. It is clear that the Ni/G/ZnO sample exhibits a higher

removal percentage than the other samples (almost double) in both time periods, thus improving both adsorption and degradation of the contaminant. The Ni foam and Ni/G foam are characterized by their abundance of microscopic-sized pores, which provide a large surface area leading to high contaminants adsorption capacity. The significant enhancement in adsorption observed in the samples with G/ZnO can be attributed to two concurrent factors. Firstly, the morphology of the deposited ZnO increases the contact surface, thereby facilitating increased adsorption. This fact is corroborated by SEM images **(Figures 7** and **9)**, where the nanostructured feature of ZnO is clearly appreciated. Secondly, the pH of the MB solution is 6, which results in the formation of $Zn(OH)^+$ on the ZnO surface. In contrast, the functional groups of MB carry a negative charge ($-SO3^-$). This allows the formation of an ionic bond that increases the adsorption capacity [69].

Figure 12 shows percentages of MB removal from the solution achieved for each sample after irradiation with UV light, represented by the black and green curves in **Figure 11**. Numerous studies [18,70,71] have corroborated that ZnO serves as a photocatalyst in this reaction. It is particularly noteworthy that the sample composed of Ni/G/ZnO exhibits the greatest efficiency, achieving about 60% removal of MB from the solution.

Table 1. MB removal percentages from the solution for each sample before and after light irradiation.

Sample	MB removal without light [%]	MB removal with light [%]
Ni	24	10
Ni/G	20	14
Ni/ZnO	20	14
Ni/G/ZnO	41	28

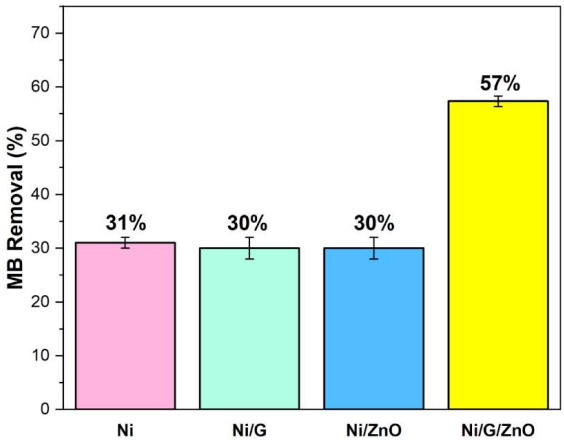

Figure 12. Percent removal of MB achieved by the different samples.

4. Discussion

This work reports on the growth of ZnO on Ni and Ni/G foams by electrodeposition and its possible application in the removal of dyes in water bodies. In the case of bare Ni foam, ZnO deposition is evidenced by the presence of Zn in EDS analysis, although ZnO growth could not be observed by XRD. On the other hand,

when the Ni/G foam is used as a substrate, a large amount of ZnO deposition is observed by both techniques used. Unlike the work of Fei et al. [30], here, the growth of ZnO was achieved in a single step, without the need of adding seeds and performing heat treatments. This behavior could be due to the presence of defects and wrinkles in the graphene, which act as nucleation sites for ZnO. Then growth occurs in all directions.

It is worth highlighting that our starting solution has a low concentration of precursors compared to the growth solution used by Lv et al. [64]. The salt that contains the Zn^{2+}, $Zn(NO_3)_2$, has a concentration 20 times lower, while the supporting electrolyte KCl has a concentration 48 times lower. This makes our process more affordable and accessible. Furthermore, the application of a potential difference of −800 mV in our synthesis results in a more efficient and less demanding method in terms of equipment compared to the use of −10 V in the aforementioned study.

Regarding the incorporation of graphene, two benefits were found: in addition to allowing nucleation at lower applied voltages, it increases the percentage of MB removal from the solution (57%). In this context, it is interesting to note that graphene is an organic, non-toxic, and inexpensive material. The results obtained in this work are close to those obtained by various authors who grow ZnO on different substrates [3,72]. Fei et al. [30] do photocatalysis and photoelectrocatalysis using the Ni/ZnO and Ni/ZnO/MoS_2 heterojunction. The results obtained with both techniques with the Ni/ZnO electrode are less efficient than our findings doing photocatalysis with the Ni/G/ZnO heterostructure. However, Fei and co-workers achieved higher removal when using the Ni/ZnO/MoS_2 heterostructure, although it should be noted that graphene is a less toxic and cheaper compound.

On the other hand, Kulis-Kapuscinska et al. [10] have studied the photodegradation of MB by growing ZnO films by sputtering on Si(100) with a subsequent thermal treatment and have managed to remove 64% of MB from the solution in 540 min. That is, with a more complicated growth method they have achieved a result similar to that obtained in this work with a substantial difference in time: their experiment lasts 9 h while ours lasts 3 h, reducing the cost involved in maintaining the light on. This result is very important from the point of view that the degradation rate is usually a limiting factor for the selection of the photocatalyst. This could be due, in addition to the graphene, to the chosen substrate, since the Ni foam, being so porous, has a large active surface.

The improvements occur mainly due to the use of a nickel foam that increases the active surface compared to other flat substrates [30], added to the incorporation of graphene, which inhibits the recombination of electrons and holes according to the mechanism that can be seen in **Figure 13**. The conduction band of ZnO (−4.05 eV vs. vacuum) is aligned with the graphene in such a way that the electron excited in the semiconductor can be transferred to the graphene (also taking advantage of the high electron mobility), separating the charges and reducing, thus way, recombination. Then, the electron and the hole interact with the water in the solution: the molecular oxygen is reduced, generating the superoxide anion O_2^- and the water is oxidized to obtain hydroxyl radicals (OH*), which finally degrade the MB, and CO_2 and H_2O are obtained as products of this [59,62,73].

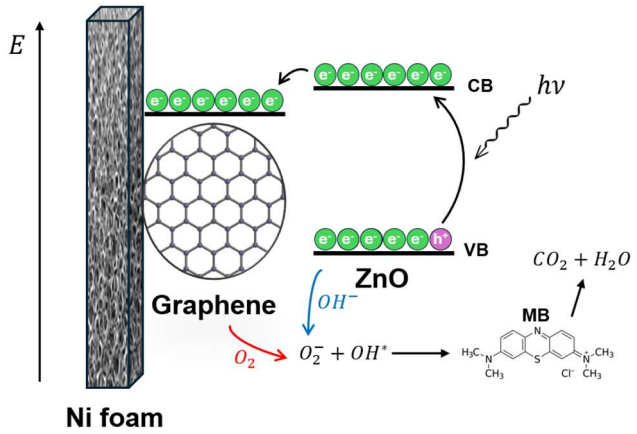

Figure 13. Scheme of the process with the ZnO and graphene bands.

5. Conclusion

In this study, ZnO was successfully electrodeposited on Ni/G foam substrates to obtain new materials with high specific surface area. Large amounts of ZnO were observed on Ni/G due to the presence of graphene, whose defects acted as nucleation sites. SEM images confirmed a homogeneous distribution of ZnO nanorods along the substrate. Instead, scarce deposition was observed for the bare Ni foam. The combined presence of ZnO and graphene increased the MB removal capacity, giving around 60% higher than what is achieved with the other heterostructures. The percentage improvement in terms of adsorption is due to the ionic bond that occurs between the ZnO surface and the negatively charged functional groups of the MB, while in photocatalysis it is probably due to a decrease in electron/hole recombination that leads to better charge separation.

Furthermore, the electrodeposition technique is a highly scalable method, so the synergistic effects of G/ZnO heterojunctions on a porous substrate become an interesting alternative for outperforming in areas of water cleaning and environmental remediation.

This study highlights the importance of the efficient synthesis of ZnO on Ni/G substrates via electrodeposition, not only for its applications in environmental remediation but also for its contribution to the development of sustainable practices within the framework of green chemistry.

Author contributions: Conceptualization, LCD; methodology, LCD, LFM, MVG; validation, LCD, MVG and LFM; formal analysis, LFM and LJ; investigation, LFM; resources, LCD, FJI and MM; data curation, LFM, MVG and LJ; writing—original draft preparation, LCD and LFM; writing—review and editing, LCD, FJI, LFM and MVG; visualization, LFM; supervision, LCD and FJI; project administration, LCD and MM; funding acquisition, LCD and FJI. All authors have read and agreed to the published version of the manuscript.

Funding: This research was funded by CONICET, grant numbers PIP0901 and PIP 0001 and UNLP grant numbers 11X933 and X-887.

Acknowledgments: LFM, MVG, LJ, MM, FJI and LCD are members of CONICET, Argentina. The authors acknowledge Sebastian Rabal, technical personnel of

CONICET, for technical assistance in the electrodeposition method. The authors also acknowledge the members of the Sensors and Electrocatalysis research group at INIFTA, for the growth of CVD graphene.

Conflict of interest: The authors declare no conflict of interest.

References

1. Xu X, Yang H, Li C. Theoretical Model and Actual Characteristics of Air Pollution Affecting Health Cost: A Review. International Journal of Environmental Research and Public Health. 2022; 19(6): 3532. doi: 10.3390/ijerph19063532
2. Lin L, Yang H, Xu X. Effects of Water Pollution on Human Health and Disease Heterogeneity: A Review. Frontiers in Environmental Science. 2022; 10. doi: 10.3389/fenvs.2022.880246
3. Lanjwani MF, Tuzen M, Khuhawar MY, et al. Trends in photocatalytic degradation of organic dye pollutants using nanoparticles: A review. Inorganic Chemistry Communications. 2024; 159: 111613. doi: 10.1016/j.inoche.2023.111613
4. Saleh TA. Advanced Nanomaterials for Water Engineering, Treatment, and Hydraulics. IGI Global; 2017.
5. Gupta VK, Mohan D, Suhas, et al. Removal of 2-Aminophenol Using Novel Adsorbents. Industrial & Engineering Chemistry Research. 2006; 45(3): 1113-1122. doi: 10.1021/ie051075k
6. Saleh TA. Mercury sorption by silica/carbon nanotubes and silica/activated carbon: a comparison study. Journal of Water Supply: Research and Technology - Aqua. 2015; 64(8): 892-903. doi: 10.2166/aqua.2015.050
7. Bin-Dahman OA, Saleh TA. Synthesis of polyamide grafted on biosupport as polymeric adsorbents for the removal of dye and metal ions. Biomass Conversion and Biorefinery. 2022; 14(2): 2439-2452. doi: 10.1007/s13399-022-02382-8
8. Crini G. Non-conventional low-cost adsorbents for dye removal: A review. Bioresource Technology. 2006; 97(9): 1061-1085. doi: 10.1016/j.biortech.2005.05.001
9. Lellis B, Fávaro-Polonio CZ, Pamphile JA, et al. Effects of textile dyes on health and the environment and bioremediation potential of living organisms. Biotechnology Research and Innovation. 2019; 3(2): 275-290. doi: 10.1016/j.biori.2019.09.001
10. Kulis-Kapuscinska A, Kwoka M, Borysiewicz MA, et al. Photocatalytic degradation of methylene blue at nanostructured ZnO thin films. Nanotechnology. 2023; 34(15): 155702. doi: 10.1088/1361-6528/aca910
11. Begum R, Najeeb J, Sattar A, et al. Chemical reduction of methylene blue in the presence of nanocatalysts: a critical review. Reviews in Chemical Engineering. 2019; 36(6): 749-770. doi: 10.1515/revce-2018-0047
12. American Association of Textile Chemists and Colorists. Color technology in the textile industry, 2nd ed. Amer Assn of Textile; 1997.
13. Varjani S, Rakholiya P, Shindhal T, et al. Trends in dye industry effluent treatment and recovery of value added products. Journal of Water Process Engineering. 2021; 39: 101734. doi: 10.1016/j.jwpe.2020.101734
14. Senobari S, Nezamzadeh-Ejhieh A. A comprehensive study on the enhanced photocatalytic activity of CuO-NiO nanoparticles: Designing the experiments. Journal of Molecular Liquids. 2018; 261: 208-217. doi: 10.1016/j.molliq.2018.04.028
15. Yazdani O, Irandoust M, Ghasemi JB, et al. Thermodynamic study of the dimerization equilibrium of methylene blue, methylene green and thiazole orange at various surfactant concentrations and different ionic strengths and in mixed solvents by spectral titration and chemometric analysis. Dyes and Pigments. 2012; 92(3): 1031-1041. doi: 10.1016/j.dyepig.2011.07.006
16. Pereira AGB, Rodrigues FHA, Paulino AT, et al. Recent advances on composite hydrogels designed for the remediation of dye-contaminated water and wastewater: A review. Journal of Cleaner Production. 2021; 284: 124703. doi: 10.1016/j.jclepro.2020.124703
17. Muzammal S, Ahmad A, Sheraz M, et al. Polymer-supported nanomaterials for photodegradation: Unraveling the methylene blue menace. Energy Conversion and Management: X. 2024; 22: 100547. doi: 10.1016/j.ecmx.2024.100547
18. Khan I, Saeed K, Zekker I, et al. Review on Methylene Blue: Its Properties, Uses, Toxicity and Photodegradation. Water. 2022; 14(2): 242. doi: 10.3390/w14020242
19. Radoor S, Karayil J, Jayakumar A, et al. Efficient removal of dyes, heavy metals and oil-water from wastewater using electrospun nanofiber membranes: A review. Journal of Water Process Engineering. 2024; 59: 104983. doi: 10.1016/j.jwpe.2024.104983
20. Rafatullah Mohd, Sulaiman O, Hashim R, et al. Adsorption of methylene blue on low-cost adsorbents: A review. Journal of

Hazardous Materials. 2010; 177(1-3): 70-80. doi: 10.1016/j.jhazmat.2009.12.047
21. Yaseen M, Khan A, Humayun M, et al. Fabrication and characterization of CuO–SiO_2/PVA polymer nanocomposite for effective wastewater treatment and prospective biological applications. Green Chemistry Letters and Reviews. 2024; 17(1). doi: 10.1080/17518253.2024.2321251
22. Buthiyappan A, Abdul Aziz AR, Wan Daud WMA. Recent advances and prospects of catalytic advanced oxidation process in treating textile effluents. Reviews in Chemical Engineering. 2016; 32(1): 1-47. doi: 10.1515/revce-2015-0034
23. Chan SHS, Yeong Wu T, Juan JC, et al. Recent developments of metal oxide semiconductors as photocatalysts in advanced oxidation processes (AOPs) for treatment of dye waste-water. Journal of Chemical Technology & Biotechnology. 2011; 86(9): 1130-1158. doi: 10.1002/jctb.2636
24. Herrmann JM. Heterogeneous photocatalysis: fundamentals and applications to the removal of various types of aqueous pollutants. Catalysis Today. 1999; 53: 115-29.
25. Lee YY, Moon JH, Choi YS, et al. Visible-Light Driven Photocatalytic Degradation of Organic Dyes over Ordered Mesoporous CdxZn1–xS Materials. The Journal of Physical Chemistry C. 2017; 121(9): 5137-5144. doi: 10.1021/acs.jpcc.7b00038
26. Saleh TA. Nanocomposite of carbon nanotubes/silica nanoparticles and their use for adsorption of Pb(II): from surface properties to sorption mechanism. Desalination and Water Treatment. 2015; 57(23): 10730-10744. doi: 10.1080/19443994.2015.1036784
27. Ravishankar TN, Manjunatha K, Ramakrishnappa T, et al. Comparison of the photocatalytic degradation of trypan blue by undoped and silver-doped zinc oxide nanoparticles. Materials Science in Semiconductor Processing. 2014; 26: 7-17. doi: 10.1016/j.mssp.2014.03.027
28. Jasso-Salcedo AB, Palestino G, Escobar-Barrios VA. Effect of Ag, pH, and time on the preparation of Ag-functionalized zinc oxide nanoagglomerates as photocatalysts. Journal of Catalysis. 2014; 318: 170-178. doi: 10.1016/j.jcat.2014.06.008
29. Wang Y, Wang Q, Zhan X, et al. Visible light driven type II heterostructures and their enhanced photocatalysis properties: a review. Nanoscale. 2013; 5(18): 8326. doi: 10.1039/c3nr01577g
30. Fei W, Li H, Li N, et al. Facile fabrication of ZnO/MoS_2 p-n junctions on Ni foam for efficient degradation of organic pollutants through photoelectrocatalytic process. Solar Energy. 2020; 199: 164-172. doi: 10.1016/j.solener.2020.02.037
31. Mustajab MA, Winata T, Arifin P. Lithium doping effect on microstructural and electrical properties of zinc oxide thin film grown by metal-organic chemical vapor deposition. Journal of Physics: Conference Series. 2022; 2243(1): 012054. doi: 10.1088/1742-6596/2243/1/012054
32. Bui QC, Ardila G, Roussel H, et al. Tuneable polarity and enhanced piezoelectric response of ZnO thin films grown by metal–organic chemical vapour deposition through the flow rate adjustment. Materials Advances. 2022; 3(1): 498-513. doi: 10.1039/d1ma00921d
33. Imran M, Ahmad R, Afzal N, et al. Copper ion implantation effects in ZnO film deposited on flexible polymer by DC magnetron sputtering. Vacuum. 2019; 165: 72-80. doi: 10.1016/j.vacuum.2019.04.010
34. Ghalmi L, Bensmaine S, Merzouk CEH. Structural Characterization of ZnO Thin Films Deposited onto Silicon Substrates using Cathodic Magnetron Sputtering. Journal of Renewable Energies. 2023; 26(1). doi: 10.54966/jreen.v26i1.1116
35. Mathew JA, Tsiumra V, Sajkowski JM, et al. Photoluminescence of Europium in ZnO and ZnMgO thin films grown by Molecular Beam Epitaxy. Journal of Luminescence. 2022; 251: 119167. doi: 10.1016/j.jlumin.2022.119167
36. Kennedy OW, Coke ML, White ER, et al. MBE growth and morphology control of ZnO nanobelts with polar axis perpendicular to growth direction. Materials Letters. 2018; 212: 51-53. doi: 10.1016/j.matlet.2017.10.017
37. Chander Joshi B, Chaudhri AK. Sol–Gel-Derived Cu-Doped ZnO Thin Films for Optoelectronic Applications. ACS Omega. 2022; 7(25): 21877-21881. doi: 10.1021/acsomega.2c02040
38. Rabeel M, Javed S, Khan R, et al. Controlling the Wettability of ZnO Thin Films by Spray Pyrolysis for Photocatalytic Applications. Materials. 2022; 15(9): 3364. doi: 10.3390/ma15093364
39. Badawi A, Althobaiti MG, Ali EE, et al. A comparative study of the structural and optical properties of transition metals (M = Fe, Co, Mn, Ni) doped ZnO films deposited by spray-pyrolysis technique for optoelectronic applications. Optical Materials. 2022; 124: 112055. doi: 10.1016/j.optmat.2022.112055
40. Donderis V, Orozco J, Cembrero J, et al. Doped Nanostructured Zinc Oxide Films Grown by Electrodeposition. Journal of Nanoscience and Nanotechnology. 2010; 10(2): 1387-1392. doi: 10.1166/jnn.2010.1869
41. Lghazi Y, Bahar J, Youbi B, et al. Nucleation/Growth and Optical Proprieties of Co-doped ZnO Electrodeposited on ITO

Substrate. Biointerface Research in Applied Chemistry. 2021; 12(5): 6776-6787. doi: 10.33263/briac125.67766787
42. Reyes Tolosa MD, Alajami M, Montero Reguera AE, et al. Influence of seed layer thickness on properties of electrodeposited ZnO nanostructured films. SN Applied Sciences. 2019; 1(10). doi: 10.1007/s42452-019-1293-7
43. Nedzinskas R, Suchodolskis A, Trinkler L, et al. Optical characterization of high-quality ZnO (0002) / Cu (111) epilayers grown by electrodeposition. Optical Materials. 2023; 138: 113650. doi: 10.1016/j.optmat.2023.113650
44. Chatterjee S, Kar AK. Precursor concentration induced nanostructural evolution of electrodeposited ZnO thin films and its effect on their optical and photocatalytic properties. Journal of Materials Science: Materials in Electronics. 2021; 33(11): 8970-8986. doi: 10.1007/s10854-021-07010-1
45. Lim HC, Park E, Shin I, et al. Electrodeposition of Zinc Oxide Nanowires as a Counter Electrode in Electrochromic Devices. Bulletin of the Korean Chemical Society. 2020; 41(3): 358-361. doi: 10.1002/bkcs.11953
46. Kim H, Moon JY, Lee HS. Effect of $ZnCl_2$ concentration on the growth of ZnO by electrochemical deposition. Current Applied Physics. 2012; 12: S35-S38. doi: 10.1016/j.cap.2012.05.036
47. Haga H, Jinnai M, Ogawa S, et al. Rapid fabrication of ZnO film by electrochemical deposition method from aqueous solution. Electrical Engineering in Japan. 2021; 214(2). doi: 10.1002/eej.23320
48. Yamabi S, Imai H. Growth conditions for wurtzite zinc oxide films in aqueous solutions. Journal of Materials Chemistry. 2002; 12(12): 3773-3778. doi: 10.1039/b205384e
49. Londhe PU, Chaure NB. Effect of pH on the properties of electrochemically prepared ZnO thin films. Materials Science in Semiconductor Processing. 2017; 60: 5-15. doi: 10.1016/j.mssp.2016.12.005
50. Xu L, Guo Y, Liao Q, et al. Morphological Control of ZnO Nanostructures by Electrodeposition. The Journal of Physical Chemistry B. 2005; 109(28): 13519-13522. doi: 10.1021/jp051007b
51. El-Shamy A, Elsayed E, Eessaa A, et al. Fabrication, characterization and monitoring the propagation of nanocrystalline zno thin film on ito substrate using electrodeposition technique. Egyptian Journal of Chemistry. 2022. doi: 10.21608/ejchem.2022.126134.5595
52. Liu WL, Chang YC, Hsieh SH, Chen WJ. Effects of Anions in Electrodeposition Baths on Morphologies of Zinc Oxide Thin Films. International Journal of Electrochemical Science. 2013; 8: 983-90.
53. Ghannam H, Bazin C, Chahboun A, et al. Control of the growth of electrodeposited zinc oxide on FTO glass. CrystEngComm. 2018; 20(41): 6618-6628. doi: 10.1039/c8ce01223g
54. Cembrero J, Busquets-Mataix D. ZnO crystals obtained by electrodeposition: Statistical analysis of most important process variables. Thin Solid Films. 2009; 517(9): 2859-2864. doi: 10.1016/j.tsf.2008.10.069
55. Urade AR, Lahiri I, Suresh KS. Graphene Properties, Synthesis and Applications: A Review. JOM. 2022; 75(3): 614-630. doi: 10.1007/s11837-022-05505-8
56. Jain P, Rajput RS, Kumar S, et al. Recent Advances in Graphene-Enabled Materials for Photovoltaic Applications: A Comprehensive Review. ACS Omega. 2024; 9(11): 12403-12425. doi: 10.1021/acsomega.3c07994
57. Yang H, Li J, Yu D, et al. Seed/Catalyst Free Growth and Self-Powered Photoresponse of Vertically Aligned ZnO Nanorods on Reduced Graphene Oxide Nanosheets. Crystal Growth & Design. 2016; 16(9): 4831-4838. doi: 10.1021/acs.cgd.6b00034
58. Messina MM, Picone AL, dos Santos Claro PC, et al. Graphene Grown on Ni Foam: Molecular Sensing, Graphene-Enhanced Raman Scattering, and Galvanic Exchange for Surface-Enhanced Raman Scattering Applications. The Journal of Physical Chemistry C. 2018; 122(16): 9152-9161. doi: 10.1021/acs.jpcc.7b12021
59. Gao C, Zhong K, Fang X, et al. Brief Review of Photocatalysis and Photoresponse Properties of ZnO–Graphene Nanocomposites. Energies. 2021; 14(19): 6403. doi: 10.3390/en14196403
60. Singh P, Shandilya P, Raizada P, et al. Review on various strategies for enhancing photocatalytic activity of graphene based nanocomposites for water purification. Arabian Journal of Chemistry. 2020; 13(1): 3498-3520. doi: 10.1016/j.arabjc.2018.12.001
61. Yoo DH, Cuong TV, Luan VH, et al. Photocatalytic Performance of a Ag/ZnO/CCG Multidimensional Heterostructure Prepared by a Solution-Based Method. The Journal of Physical Chemistry C. 2012; 116(12): 7180-7184. doi: 10.1021/jp210216w
62. Cai R, Wu J gen, Sun L, et al. 3D graphene/ZnO composite with enhanced photocatalytic activity. Materials & Design. 2016; 90: 839-844. doi: 10.1016/j.matdes.2015.11.020
63. Messina MM, Coustet ME, Ubogui J, et al. Simultaneous Detection and Photocatalysis Performed on a 3D Graphene/ZnO Hybrid Platform. Langmuir. 2020; 36(9): 2231-2239. doi: 10.1021/acs.langmuir.9b03502

64. Lv S, Geng P, Wang H, et al. In Situ Construction of ZnO/Ni_2S_3 Composite on Ni Foam by Combing Potentiostatic Deposition with Cyclic Voltammetric Electrodeposition. Micromachines. 2021; 12(7): 829. doi: 10.3390/mi12070829
65. Zhong Y, Yang S, Fang Y, et al. In situ constructing Ni foam supported ZnO-CdS nanorod arrays for enhanced photocatalytic and photoelectrochemical activity. Journal of Alloys and Compounds. 2021; 868: 159187. doi: 10.1016/j.jallcom.2021.159187
66. Miao F, Wu W, Miao R, et al. Graphene/nano-ZnO hybrid materials modify Ni-foam for high-performance electrochemical glucose sensors. Ionics. 2018; 24(12): 4005-4014. doi: 10.1007/s11581-018-2539-x
67. Abbas SI, Alattar AM, Al-Azawy AA. Enhanced ultraviolet photodetector based on Al-doped ZnO thin films prepared by spray pyrolysis method. Journal of Optics. 2023; 53(1): 396-403. doi: 10.1007/s12596-023-01164-3
68. Bidault F, Brett DJL, Middleton PH, et al. A new application for nickel foam in alkaline fuel cells. International Journal of Hydrogen Energy. 2009; 34(16): 6799-6808. doi: 10.1016/j.ijhydene.2009.06.035
69. Zhang F, Lan J, Yang Y, et al. Adsorption behavior and mechanism of methyl blue on zinc oxide nanoparticles. Journal of Nanoparticle Research. 2013; 15(11). doi: 10.1007/s11051-013-2034-2
70. He X, Yang Y, Li Y, et al. Effects of structure and surface properties on the performance of ZnO towards photocatalytic degradation of methylene blue. Applied Surface Science. 2022; 599: 153898. doi: 10.1016/j.apsusc.2022.153898
71. Waghchaure RH, Adole VA, Jagdale BS. Photocatalytic degradation of methylene blue, rhodamine B, methyl orange and Eriochrome black T dyes by modified ZnO nanocatalysts: A concise review. Inorganic Chemistry Communications. 2022; 143: 109764. doi: 10.1016/j.inoche.2022.109764
72. Prerna, Agarwal H, Goyal D. Photocatalytic degradation of textile dyes using phycosynthesised ZnO nanoparticles. Inorganic Chemistry Communications. 2022; 142: 109676. doi: 10.1016/j.inoche.2022.109676
73. Saleh TA, Gondal MA, Drmosh QA. Preparation of a MWCNT/ZnO nanocomposite and its photocatalytic activity for the removal of cyanide from water using a laser. Nanotechnology. 2010; 21(49): 495705. doi: 10.1088/0957-4484/21/49/495705